Dynamics of Charge-Transfer-to-Solvent Precursor States in $I^-(water)_n$ ($n = 3-10$) Clusters Studied with Photoelectron Imaging†

Aster Kammrath, Jan R. R. Verlet, Arthur E. Bragg, Graham B. Griffin, and Daniel M. Neumark*

Department of Chemistry, University of California, Berkeley, California 94720, and Chemical Sciences Division, Lawrence Berkeley National Laboratory, Berkeley, California 94720

Received: June 23, 2005; In Final Form: September 1, 2005

The dynamics of charge-transfer-to-solvent states are studied in $I^-(H_2O)_{n=3-10}$ clusters and their deuterated counterparts using time-resolved photoelectron imaging. The photoelectron spectra for clusters with $n \geq 5$ reveal multiple time scales for dynamics after their electronic excitation. An increase in the vertical detachment energy (VDE) by several hundred millielectronvolts on a time scale of ∼1 ps is attributed to stabilization of the excess electron, primarily through rearrangement of the solvent molecules, but a contribution to this stabilization from motion of the I atom cannot be ruled out. The VDE drops by ∼50 meV on a time scale of tens of picoseconds; this is attributed to loss of the neutral iodine atom. Finally, the pump−probe signal decays with a time constant of 60 ps−3 ns, increasing with cluster size. This decay is commensurate with the growth of very slow electrons and is attributed to autodetachment. Smaller clusters ($n = 3, 4$) display simpler dynamics. Anisotropy parameters are reported for clusters $n = 4-9$.

1. Introduction

An increasingly important area in the field of cluster science focuses on understanding how phenomena associated with bulk systems are manifested in finite clusters. The broad range of chemical and physical phenomena associated with aqueous solutions represent a uniquely rich opportunity for this type of study, motivating numerous spectroscopic studies of neutral[1] and charged[2] water clusters. Water clusters doped with halide anions are a particularly interesting subclass of charged water clusters, as their vibrational spectroscopy reveals how solvation of the anion competes with the strong hydrogen bonding among water molecules,[3] while their electronic spectroscopy probes the interaction of diffuse electrons with the solvent network.[4,5] This paper focuses on the latter topic: we use time-resolved photoelectron imaging to monitor the dynamics subsequent to excitation of the charge-transfer-to-solvent (CTTS) band in $I^-(H_2O)_n$ clusters.

CTTS states were first observed in 1928[6] when a solution of aqueous iodide exhibited two broad absorption bands in the UV. Iodide has no electronically bound excited states, while a single water molecule cannot accommodate an excess electron. The absorption was thus attributed to a transition in which an electron is ejected from the halide into a state defined by the collective action of the solvent molecules. The same phenomenon has been observed for other anions in polar solvents, and has been demonstrated as an elegant means of generating solvated electrons.[7]

The CTTS states are a sensitive probe of local solvent structures. Due to this fact and to the importance of solvated electrons in many fields of chemistry, such as electron transfer, radiation chemistry, and atmospheric thermodynamics, CTTS states have been extensively studied both by experimental and theoretical methods. Much of the early work is summarized in the review of Blandamer and Fox.[8]

In the early 1990s, Eisenthal and co-workers carried out femtosecond time-resolved studies of the CTTS state formed by multiphoton excitation of aqueous iodide solutions.[9] Similar experiments were carried out on aqueous chloride solutions by Gauduel.[10] This experimental work was complemented by quantum molecular dynamics simulations by Sheu and Rossky[11] and by Staib and Borgis.[12,13] Dynamics following resonant single photon excitation to the lowest CTTS state in the same system were studied by Bradforth and co-workers,[14−16] and more recently by Laubereau and co-workers, who studied the temperature dependence of the dynamics observed.[17] They interpreted their results according to the model suggested by the theoretical work of Staib and Borgis on the related system of aqueous chloride. That is, excitation is followed by the formation of a halogen:electron pair which may undergo geminate recombination or else dissociate to produce a hydrated electron. The experimental results show that, in the case of aqueous iodide, short-range ejection of the electron to the $I{:}e^-$ pair occurs within 200 fs, followed by stabilization of the contact pair via solvent rearrangement, complete within ∼2 ps. Geminate recombination takes place with a lifetime on the order of 30 ps, with ∼25% of electrons undergoing diffusive escape with an upper limit lifetime of ∼70 ps.[16] Both solvation and recombination rates are found to be temperature-dependent, slowing as the solution is cooled.[17]

The question of the number of solvent molecules needed to support a CTTS state was addressed by Serxner and co-workers,[4] who studied the absorption spectra of $I^-(H_2O)_{n=1-4}$. They observed a maximum at a photon energy of ∼3.9 eV for the $I^-(H_2O)_2$ cluster that moves to higher energies with increasing cluster size. This absorption was assigned to the cluster precursor to the lower of the bulk CTTS states (based on the iodine $^2P_{3/2}$ state), which has its maximum absorption ∼5.5 eV above the ground state.[8] Ab initio studies by Chen and Sheu[18] and Lee and Kim[19] also recover evidence of this precursor state, as well as a second one at higher excitation energy starting in clusters

* Corresponding author. E-mail: dneumark@berkeley.edu.
† Part of the special issue "Jack Simons Festschrift".

10.1021/jp053422+ CCC: $30.25 © 2005 American Chemical Society
Published on Web 10/14/2005

as small as $I^-(H_2O)_4$. The relationship between CTTS excitation in clusters and in bulk water was examined by Bradforth and Jungwirth.[5]

Lehr et al.[20] performed the first experimental time-resolved study of excitation dynamics in the cluster precursor to CTTS states for $I^-(H_2O)_{n=4-6}$ and their deuterated counterparts, using time-resolved photoelectron spectroscopy with a magnetic bottle photoelectron energy analyzer. They observed a shift to higher vertical detachment energy (VDE) at early pump−probe delays for $n = 5$ and 6, accompanied by an increase in photodetachment signal, which they interpreted as solvent rearrangement resulting in stabilization of the electron in a state localized on the water cluster. Subsequently, the transient exhibited simple exponential decay on a time scale of picoseconds, which was attributed to excited state autodetachment. Similar results were seen for larger iodide−water clusters as well as in clusters with halides complexed to other solvent species.[21−23]

Theoretical modeling of the dynamics was carried out by Chen and Sheu,[24,25] who pointed out that Lehr et al. had neglected the effect of the neutral iodine atom in their interpretation. Chen and Sheu attributed the shift in VDE to loss of the neutral iodine atom, but treated the solvent moiety as frozen in the same configuration as in the original $I^-(H_2O)_n$ cluster. More recent work by Jordan,[26] Peslherbe,[27] and Kim[28,29] suggests that both the iodine and solvent motion must be taken into account if an accurate picture is to be achieved.

In the current study we probe the dynamics of CTTS excitation in $I^-(H_2O)_{n=3-10}$ and their deuterated counterparts by time-resolved photoelectron imaging, with attention both to the short-time dynamics observed by Lehr et al. for clusters $n = 4-6$,[20] and to the long-time decay of the population. We present evidence in support of short-time solvent rearrangement, leading to stabilization of the excess electron, and we observe slower dynamics that we attribute to loss of the neutral iodine atom. In contrast to the previous study, we are able to observe the low-energy portion of the photoelectron spectrum and do, in fact, observe low-energy photoelectrons from autodetachment, which display depletion dynamics mirroring the growth and decay of pump−probe signal. Time scales for all processes are determined. We also report anisotropy parameters for CTTS state detachment from all clusters studied.

2. Experimental Section

Our experimental apparatus has been described in detail elsewhere,[30] so only pertinent details will be given here. Argon gas at 15−20 psi is passed over a reservoir of CH_3I and through a bubbler filled with water, finally undergoing supersonic expansion into vacuum, through either a standard piezo valve pulsed at 500 Hz (for all H_2O clusters as well as $I^-(D_2O)_{n=5-7}$) or an Even-Lavie solenoid valve[31] pulsed at 100 Hz (for $I^-(D_2O)_{n=3-10}$). The molecular beam is crossed with an electron beam at 1200 eV (200−400 eV in the case of the Even-Lavie valve) to produce negative ions by secondary electron attachment. The ions are then perpendicularly extracted into a Wiley-McLaren type mass spectrometer.[32] The cluster of interest is mass-selected and isolated using an electrostatic switch which also serves as a re-referencing tube and the first plate of the velocity map imaging (VMI) lens.[33] The mass-selected ion packet is crossed with the laser pump and probe beams, and the resulting photoelectron cloud is projected in two dimensions on a 70 mm dual multichannel plate coupled to a phosphor screen. Images from the phosphor screen are recorded by a charge-coupled device (CCD) camera.

The fundamental and third harmonic of a chirped-pulse amplified Ti:sapphire femtosecond oscillator (Clark-MXR, NJA-5, CPA-1000) were used as the probe and pump wavelengths, respectively. The oscillator is tuned to 795 nm, and the output of the amplifier is recompressed to give 100 fs pulses. This output is split and the pump pulse is tripled in BBO yielding 20 μJ/pulse at 4.65 eV. The remaining 200 μJ/pulse at 1.56 eV is used as a probe and directed onto a computer controlled translation stage which generates the desired pump−probe delays. The beams are collinearly recombined and focused at the interaction region using a 50 cm lens.

One photoelectron is typically collected for every 1−10 laser shots, depending on cluster size, and the images are accumulated for 100 000−200 000 laser shots. The spectrometer is calibrated daily with I^-. Every third scan is set as a normalization scan near the temporal overlap of the two laser pulses (time zero), and normalization is carried out relative to the integrated intensity over all electron kinetic energies (eKE).

Images are four-way symmetrized to account for inhomogeneity in the detector, and the three-dimensional (3-D) velocity distribution is reconstructed using the basis set expansion (BASEX) method,[34] for analysis of the photoelectron spectra (PES), or the polar basis set expansion (pBASEX) method for extraction of the photoelectron angular distributions (PADS). pBASEX was not used for PES analysis, as it concentrates noise at the center of the reconstructed image, thereby interfering with analysis of low-energy electron signal.

Photoelectron spectra are obtained by radial integration of the $\varphi = 0$ slice through the reconstructed 3-D distribution, and conversion from velocity to energy space, with a typical resolution of 5%. The same 3-D slice is fitted with an even series of Legendre polynomials, truncated at $n = 2m$ for an m-photon process. The coefficients of the expansion, or anisotropy parameters, define the anisotropy of the photoelectron angular distribution (PAD) according to[35]

$$I(\theta) = (\sigma/4\pi)[1 + \beta_2 P_2(\cos\theta) + \beta_4 P_2(\cos\theta)] \qquad (1)$$

The reported vertical detachment energies (VDEs) and peak widths are found by fitting Gaussians to the individual photoelectron spectra, except for $I^-(H_2O)_{n=4,10}$ and $I^-(D_2O)_3$, where signal intensity was insufficient to allow a proper fit. In these cases the energy was determined by taking an intensity-weighted average over the peak. This method was found to give good agreement with the Gaussian-fitting procedure, so that the two methods should produce consistent results.

3. Results

Figure 1 shows one-photon photoelectron (PE) spectra of $I^-(D_2O)_{n=2-7}$ taken at a photon energy of 5.14 eV. All time-resolved studies were carried out at a lower pump photon energy, 4.65 eV, at which only those features in Figure 1 to the right of the dotted lines are accessible. These PE spectra are similar to those obtained by Markovich et al.[36] except for the sharp feature at eKE ≈ 0 that is particularly prominent for $n \geq 6$. As discussed below, this feature is from autodetachment rather than direct photodetachment. It is observed readily with our PE imaging instrument, which is much more sensitive to very low energy electrons than the magnetic bottle analyzer used in previous studies of these anions.[20,36]

3.1. Time-Resolved PE Spectra. Figures 2−4 show typical time-resolved spectra for clusters $I^-(water)_n$ with $n = 4$, 7, and 9, respectively. Electron kinetic energy (eKE) is plotted on the horizontal axis with pump−probe delay increasing from front to back. The insets show the behavior of the integrated intensity of features A (filled squares) and B (open circles) as a function

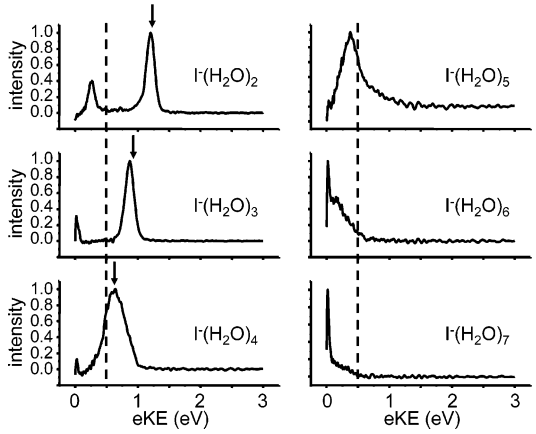

Figure 1. PES of $I^-(H_2O)_n$ taken at 5.14 eV. Dotted lines mark eKE = 0 eV for the pump laser pulse (4.65 eV) used in the time-resolved experiments reported here. Downward arrows mark the maximum of the CTTS absorbance taken from Serxner et al.[4]

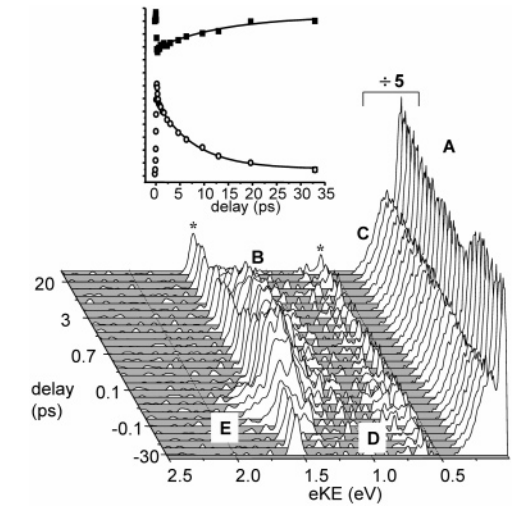

Figure 2. Time-resolved photoelectron spectrum of $I^-(D_2O)_4$. Signal intensity is plotted as a function of eKE along the horizontal axis, with pump−probe delay increasing front to back. The features marked with an asterisk (*) at 0.65 and 1.55 eV are most likely due to interference from $I^-(D_2O)_2Ar$. The inset shows the integrated intensities of features A (filled squares) and B (open circles) as a function of pump−probe delay, with fits superimposed as solid lines.

of pump−probe delay, as labeled in each figure. Results are shown for D_2O clusters, since signal-to-noise levels were somewhat better than in spectra obtained for H_2O clusters. Isotope effects are relatively minor and are discussed in more detail in section 4.2.

In Figure 2, feature C is from direct photodetachment of $I^-(D_2O)_4$ by the pump pulse, corresponding to the peak at eKE = 0.64 eV in Figure 1. The two features marked with an asterisk (*) show no time dependence and are most likely from direct detachment of $I^-(D_2O)_2 \cdot Ar$, which has the same mass.

Two additional features, D and E, are separated by the spin−orbit splitting of iodine. These features persist only as long as the cross-correlation of the pump and probe laser pulses, ~180 fs. They are assigned to pump−probe nonresonant two-photon detachment from $I^-(D_2O)_4$ to neutral clusters with the I atom in its $^2P_{3/2}$ and $^2P_{1/2}$ states, respectively. Feature E is, in fact, observed for all clusters, appearing as a shoulder at low eKE on the CTTS feature in $n = 5-10$. While its intensity in most cases is very low relative to that of the other features in the spectrum, and the peak is not so cleanly separable as in the smaller clusters, the presence of feature E in all spectra is a

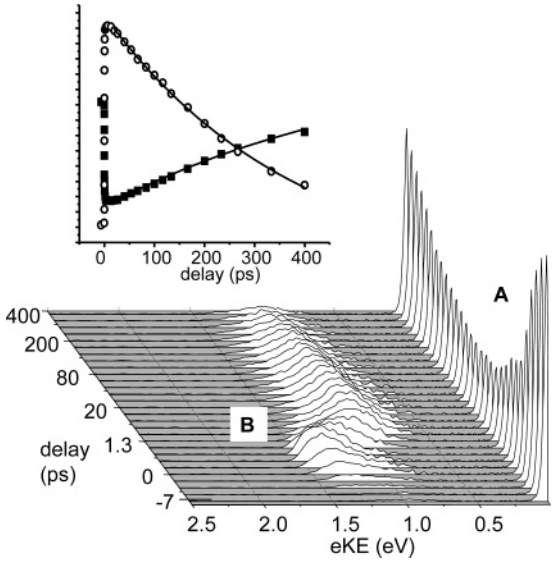

Figure 3. Time-resolved photoelectron spectrum of $I^-(D_2O)_7$. Signal intensity is plotted as a function of eKE along the horizontal axis, with pump−probe delay increasing front to back. The inset shows the integrated intensities of features A (filled squares) and B (open circles) as a function of pump−probe delay with fits superimposed as solid lines.

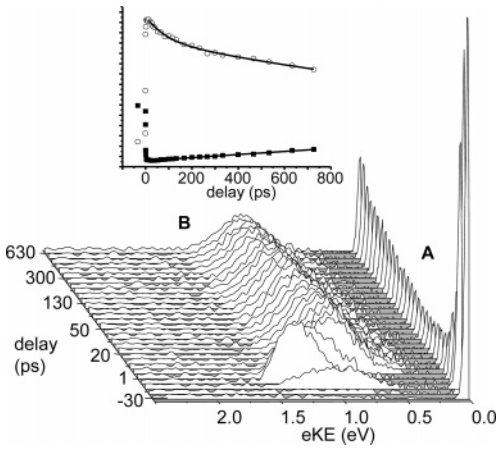

Figure 4. Time-resolved photoelectron spectrum of $I^-(D_2O)_9$. Signal intensity is plotted as a function of eKE along the horizontal axis, with pump−probe delay increasing front to back. The inset shows the integrated intensities of features A (filled squares) and B (open circles) as a function of pump−probe delay with fits superimposed as solid lines.

convenient way of determining time zero and the cross-correlation of our laser pulses in situ.

Features A and B show the most interesting time dependence. Feature B corresponds to resonant pump−probe detachment through the CTTS state, as observed by Lehr et al.[20] The integrated intensity of this signal (I_{CTTS}) continues to rise quickly through the cross-correlation, after which it begins immediately to decay. The very low energy feature A was not seen in our earlier studies using the magnetic bottle analyzer. As shown in the inset, the intensity of this feature drops abruptly at positive pump−probe delay times and recovers on approximately the same time scale over which feature B decays.

The spectrum of $n = 3$ is essentially the same as that presented for $n = 4$, but with faster decay of feature B. Also, neither feature A nor either of the time-independent features appears, and the CTTS signal is less intense relative to features D and E, consistent with the CTTS band being further from our pump wavelength.

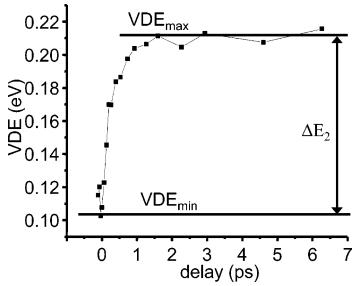

Figure 5. VDE_{CTTS} plotted as a function of pump−probe delay for $I^-(D_2O)_4$.

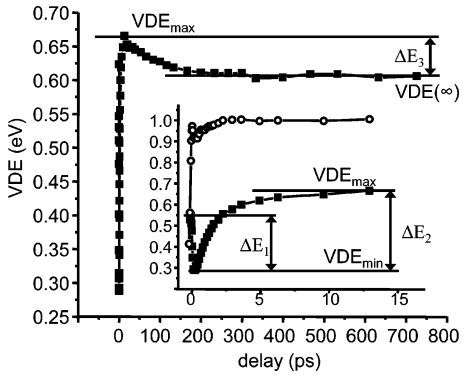

Figure 6. VDE_{CTTS} plotted as a function of pump−probe delay for $I^-(D_2O)_9$. The inset shows details of the short-time dynamics, with VDE_{CTTS} shown as filled squares and I_{CTTS} as open circles. The spike in I_{CTTS} at very early time is due to interference from feature E.

Figure 3 is taken from $I^-(D_2O)_7$ and is typical of cluster sizes $n = 5-7$ (both isotopes). Feature C no longer appears, showing that direct one-photon detachment is no longer occurring. At early times, there is a sharp rise in I_{CTTS}, accompanied by a similarly sharp drop in I_A, occurring along the rising edge of the pump−probe cross-correlation. In contrast with the $n = 4$ case, I_{CTTS} continues to rise (more slowly) over several picoseconds (and I_A continues to fall). The initial, fast rise in intensity in the region of the CTTS signal may be partly due to the rise of feature E, which cannot be cleanly distinguished from the resonant signal in most cases. However, the slower rise in I_{CTTS} continuing over 1−2 ps cannot be accounted for by cross-correlation effects, as it goes on long after the end of the pump pulse. We agree with Lehr et al.[20] that this result implies an actual increase in detachment cross section.

Figure 4 is taken from $I^-(D_2O)_9$ and is typical of cluster sizes $n \geq 8$ (both isotopes). While the short-time behavior of I_{CTTS} and I_A is similar to that in the midsize cluster range ($n = 5-7$), their long-time behavior is somewhat different. Namely, I_A no longer recovers smoothly in tandem with the decay of I_{CTTS}.

3.2. Time-Dependent VDEs. Feature B, the pump−probe feature from CTTS excitation, shows time-dependent intensity for all clusters studied here. In addition, the eKE distribution associated with this feature is time-dependent. These trends are illustrated in Figures 5 and 6, which show the vertical detachment energy, VDE_{CTTS}, as a function of pump−probe delay for $I^-(D_2O)_n$, $n = 4$ and 9. VDE_{CTTS} is defined as $h\nu - eKE_{max}$, where eKE_{max} is the electron kinetic energy corresponding to the fitted maximum intensity of feature B. The inset to Figure 6 shows details of the short-time behavior of VDE_{CTTS} (filled squares), with the various observed shifts labeled, and I_{CTTS} superimposed (open circles).

Figure 5 is taken from $I^-(D_2O)_4$. The value of VDE_{CTTS} shows little or no decrease at early time (unlike the case for larger clusters; see below), but rises quickly on the falling edge of the cross-correlation. This rise may be partly due to interference from the nonresonant peak E. However, VDE_{CTTS} continues to rise even after the end of the pump pulse, so that the total increase in VDE in this cluster, ΔE_2, cannot be attributed wholly to cross-correlation effects.

Figure 6 is taken from $I^-(D_2O)_9$ and is typical for $n = 5-10$. At early times (within the cross-correlation) VDE_{CTTS} drops sharply by ΔE_1 to VDE_{min} and then rises rapidly by ΔE_2 to VDE_{max}. ΔE_2 occurs on a time scale similar to the slow rise in I_{CTTS}, such that VDE_{max} is reached at about the same pump−probe delay as I_{CTTS} reaches its maximum value (see inset). In Figure 6, ΔE_1 and ΔE_2 are ~300 and 360 meV, respectively. At longer times, the VDE drops by ΔE_3, about 50 meV in Figure 6, to VDE(∞). The size- and time-dependent trends of these energy shifts are of considerable interest and are discussed further in sections 4 and 5.

3.3. Comparison to Bare Water Clusters. Figure 7a compares one-photon PE spectra for $(D_2O)_8^-$ with pump−probe spectra of $I^-(D_2O)_8$ at delay times corresponding to VDE_{min}, VDE_{max}, and VDE(∞). The peaks at higher and lower electron binding energies (eBEs) for $(D_2O)_8^-$ correspond to the more loosely and tightly bound isomers seen previously by Kim et al.[37] The two-photon (1 + 1′) PE spectrum of $I^-(D_2O)_8$ at VDE_{min} is quite similar to that of the more loosely bound isomer of $(D_2O)_8^-$. The PE spectra corresponding to VDE_{max} and VDE-

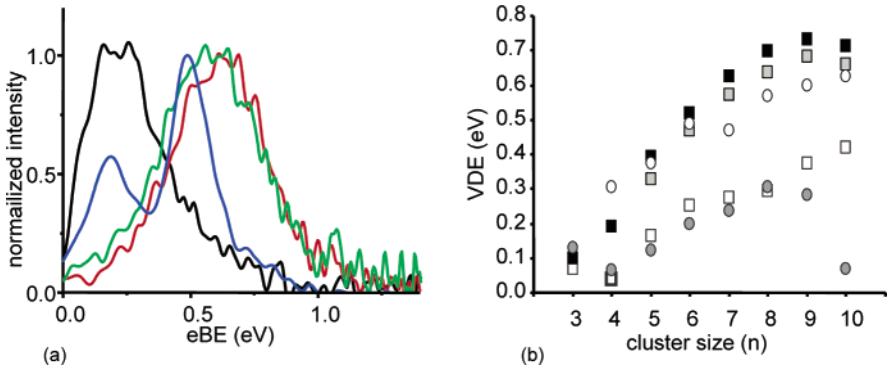

Figure 7. (a) Comparison of $I^-(D_2O)_8$ spectra at delay times corresponding to VDE_{min} (black line), VDE_{max} (red line), and VDE(∞) (green line), as labeled in Figure 6, to the spectrum of bare $(D_2O)_8^-$ (blue line). Normalized signal intensity is plotted as a function of electron binding energy (eBE). (b) Comparison of $I^-(H_2O)_n$ VDE_{min}, VDE_{max}, and VDE(∞) to the VDEs of the corresponding bare $(H_2O)_n^-$ clusters. Circles represent the two water isomers. Open squares are VDE_{min}; gray and black squares are VDE_{max} and VDE(∞), respectively, of iodide−water. The VDE for $(H_2O)_4^-$ was taken from Shin et al.,[40] and $(H_2O)_3^-$ and the weaker binding isomer of $(H_2O)_5^-$ are from Hammer et al.[41] Error bars are estimated at ±60−80 meV for $I^-(water)_n$, $n = 9-10$, and at ±30 meV for all other clusters.

TABLE 1: Lifetimes of CTTS State Population Decay (τ_d) for Cluster Sizes $n = 3-7$ and τ_{d1} and τ_{d2} for $n = 4$, 8−10, with A_1 and A_2[a]

n	τ_d (ps) H_2O/D_2O	τ_{d1} (ps) H_2O/D_2O	τ_{d2} (ps) H_2O/D_2O	A_1 H_2O/D_2O	A_2 H_2O/D_2O
3	0.59/0.70				
4	8.2/7.9			0.36/0.38	0.44/0.74
5	56/61				
6	136/131				
7	324/330				
8		81	1300	0.25	0.69
9		84	2100	0.16	0.69
10		100	3000	0.14	0.52

[a] Estimated uncertainties are ±15% for τ_d and ±30% for all other parameters.

(∞) are shifted to somewhat higher eBEs than the more strongly bound isomer of $(D_2O)_8^-$ and are broader by about a factor of 2.

Figure 7b presents a more global comparison of the vertical detachment energies (VDEs) of $I^-(H_2O)_n$ clusters to those of the corresponding bare water anion clusters.[37−40] Circles represent the two isomers of bare water anion clusters. Open, closed, and shaded squares are the VDEs of $I^-(H_2O)_n$ taken at the points corresponding to VDE_{min}, VDE_{max}, and VDE(∞), respectively, as labeled in Figures 5 and 6. For all clusters up to $n = 9$, VDE_{min} closely matches that of the more loosely bound water isomer, while for $n = 5$, 6 VDE_{max} and VDE(∞) are close to that of the more tightly bound water isomer. For $n \geq 7$, VDE_{max} exceeds the binding energy of the more stable bare water isomer by a significant margin, which remains approximately steady at 150 meV for $n = 7-9$, dropping to ∼100 meV for $n = 10$. This difference is reduced by around 50 meV for VDE(∞). Error bars are determined by the spread in data points obtained for different data sets, and are approximately 30 meV up to $n = 8$, but are 60−80 meV for $n = 9-10$.

4. Analysis

In this section, we present a more quantitative analysis of the time-dependent intensities and VDEs, with particular focus on how these dynamics depend on cluster size.

4.1. Time-Dependent Intensities. In all clusters, I_{CTTS} grows quickly, reaching a maximum within a few picoseconds. The signal then undergoes either simple exponential or biexponential decay, according to eq 2 or 3, respectively:

$$I_{CTTS}(t) = A \exp(-(t - t_0)/\tau_d) \quad (2)$$

$$I_{CTTS}(t) = A_1 \exp(-(t - t_0)/\tau_{d1}) + A_2 \exp(-(t - t_0)/\tau_{d2}) \quad (3)$$

where t is delay between the pump and probe laser pulses, t_0 is the pump−probe delay at which I_{CTTS} reaches its maximum intensity, and the τ_d's are time constants for the decay. $I^-(H_2O)_n$ clusters with $n = 3$ and 5−7 undergo simple exponential decay; corresponding constants used to fit eq 2 are summarized in Table 1. For all these clusters, the time constant for recovery of the low-energy feature A is the same as the decay constant τ_d in eq 2. For these and all other decay constants, error bars are determined by the larger of the uncertainties in the empirical fit or spread between results obtained for different data sets run for the same cluster.

For $n = 4$ and 8−10, $I_{CTTS}(t)$ decays according to eq 3. In the $n = 4$ case, however, the fast portion of the decay is most likely due to interference from the nonresonant feature E, as the time scale ($\tau_{d1} = 220-250$ fs for D_2O and H_2O, respectively) is on the same order as the fall of the cross-correlation. We thus assign the decay of I_{CTTS} solely to the second time scale, τ_{d2}, which we consequently report simply as τ_d in Table 1. The parameters used to fit these data sets are also shown in Table 1. However, for all of these clusters the recovery of feature A is described by a single exponential with time constant similar to τ_{d2}, the longer time constant in eq 3.

The decay constants τ_d and τ_{d2} increase monotonically with cluster size, ranging from 600 fs for $I^-(H_2O)_3$ to 3 ns for $I^-(H_2O)_{10}$; the highest values can be only approximately determined as the length of our delay stages prohibits following the decay dynamics to completion. For the clusters $n = 8-10$ that undergo biexponential decay, the amplitude A_1 associated with the faster time constant τ_{d1} is relatively small, around 0.2, The constants τ_{d1} are listed in Table 1 and are in the range of 80−100 ps.

4.2. Time-Dependent VDEs. As discussed in section 3, the VDEs associated with the CTTS feature for each cluster drop to VDE_{min} within the cross-correlation of the pump and probe pulses. The VDEs subsequently evolve in two different time regimes. For $t_{min} \leq t \leq t_{max}$, where t_{min} and t_{max} are the times at which the VDE is minimal and maximal, respectively, we find

$$VDE(t) = VDE_{max} - \Delta E_2 \exp(-(t - t_{min})/\tau_2)) \quad (4)$$

For $t \geq t_{max}$, we find

$$VDE(t) = VDE(\infty) + \Delta E_3 \exp(-(t - t_{max})/\tau_3) \quad (5)$$

Here τ_2 and τ_3 are the time constants for the energy shifts ΔE_2 and ΔE_3 as defined in Figure 5, and all other parameters are as designated in Figures 5 and 6. For $n = 3$, 4, only ΔE_2 is observed. For all clusters, t_{min} is ∼100 fs. Table 2 lists the rest of the parameters used to fit each cluster size to eqs 4 and 5. ΔE_1 is estimated to ±100 meV, ΔE_2 is estimated to ±30 meV, τ_2 is estimated to ±30% for $n = 3$, 4 and ±15% for larger clusters, τ_3 and t_{max} are estimated to ±20% for all clusters.

The magnitude of ΔE_2 increases monotonically with cluster size up to $n = 7$, after which there is no clear trend with cluster size. The time constant τ_2 increases with cluster size almost linearly for $n = 4-8$, after which it levels off, the values for $n = 9$ and 10 being nearly identical. No significant isotope effect is observed on the magnitude of ΔE_2 or on τ_2 for cluster sizes $n = 4-6$. This in contrast to the results of Lehr et al.,[20] who reported a delay of ∼100 fs in the start of ΔE_2 in D_2O clusters relative to H_2O. However, for $n = 7-10$, τ_2 for D_2O clusters is ∼1.2 times as large as for the corresponding H_2O clusters.

For all $I^-(H_2O)_n$ clusters, ΔE_3 is ∼50 meV. The time constant τ_3 increases with cluster size from ∼25 ps for $n = 5$ to ∼80 ps for $n = 8$, 9. Again, the largest increase occurs for $n = 5-8$. There are some differences in the values of τ_3 found for H_2O and D_2O clusters; however, they are within experimental error and τ_3 is not consistently larger for one isotope or the other.

4.3. PADs. Anisotropy parameters for features A and B (CTTS detachment) were analyzed for clusters $I^-(D_2O)_{n=4-9}$ and $I^-(H_2O)_{6,7}$. No isotope effect was observed. The anisotropy parameter β_2 in eq 1 is $\beta_2 \approx -0.15$ for feature A for all clusters. For the pump−probe detachment feature, β_2 is slightly greater than 1 for all clusters, as summarized in Table 3. Error is estimated at 15% based on comparison of several data sets taken for the same cluster on different days; it is due partly to sensitivity of the fitting routine to signal levels, and partly to imperfect polarization of the probe laser. The anisotropy parameter β_4 is close to zero for the CTTS peak in all cluster

TABLE 2: Summary of Observed Energetics, Including VDE_{min}, VDE_{max}, and VDE(∞), Magnitudes of ΔE_1 and ΔE_2, Time Constants τ_2 and τ_3, and t_{max}[a]

n	VDE_{min} (eV) H_2O/D_2O	VDE_{max} (eV) H_2O/D_2O	VDE(∞) (eV) H_2O/D_2O	ΔE_1 (meV) H_2O/D_2O	ΔE_2 (meV) H_2O/D_2O	τ_2 (fs) H_2O/D_2O	τ_3 (ps) H_2O/D_2O	t_{max} (ps)
3	0.07/0.01	0.10/0.11			30	200		
4	0.04/0.10	0.19/0.21			150/100	200/280		1
5	0.17/0.13	0.39/0.37	0.33/0.33	30	226/240	450/440	25/29	2
6	0.25/0.23	0.52/0.49	0.47/0.45	150	270/260	650/690	38/51	4
7	0.27/0.23	0.62/0.57	0.57/0.53	230	350/333	890/1110	54/73	5
8	0.29/0.23	0.70/0.60	0.64/0.57	310	400/365	1100/1300	86/77	10
9	0.37/0.30	0.73/0.65	0.68/0.61	330	360/350	1180/1470	73/90	13
10	0.42/0.37	0.71/0.69	0.66/0.66	380	290/320	1150/1430		13

[a] ΔE_1 is estimated to ±100 meV, ΔE_2 is estimated to ±30 meV, τ_2 is estimated to ±30% for $n = 3$, 4 and ±15% for larger clusters, and τ_3 and t_{max} are estimated to ±20% for all clusters. $\Delta E_3 = 50$ meV ±20 meV for all clusters (where observed).

TABLE 3: Anisotropy Parameters (β_2) for the Pump−Probe Feature in Clusters $I^-(H_2O)_{n=4-9}$[a]

n	β_2
4	1.0
5	1.4
6	1.2
7	1.2
8	1.2
9	1.0

[a] Uncertainty is estimated at ±15%.

sizes studied. No evolution of the anisotropy is observed with increasing pump−probe delay.

5. Discussion

5.1. CTTS Decay. The one-photon PE spectra in Figure 1, obtained at 5.14 eV, show an unusual dependence on cluster size. The $n = 2$ spectrum shows two peaks split by around 1 eV that are readily assigned to direct detachment to the ground state of the neutral complex, $I(^2P_{3/2})\cdot(H_2O)_2$, and the low-lying excited state $I^*(^2P_{1/2})\cdot(H_2O)_2$ in which the upper spin−orbit state of the I atom is produced. As *n* increases from 2 to 5, these spectra shift to lower eKE owing to the well-known "solvent shift"[41] that reflects the tighter binding of each additional water molecule in the anion vs the neutral cluster, so that the transition to the upper spin−orbit state is not seen at all by $n = 5$. However, the $n = 6$ and 7 spectra are dominated by an intense feature near eKE = 0. We assign this feature to resonant excitation to the CTTS state of the cluster followed by autodetachment:

$$I^-(H_2O)_n \xrightarrow{h\nu} [I^-(H_2O)_n]^* \xrightarrow{\tau_d} I\cdot(H_2O)_n + e^-, I + (H_2O)_n + e^- \quad (6)$$

The question of whether the I atom is still bound to the anion when autodetachment occurs is discussed in section 5.3.

Similarly, we assign the low-energy feature A for clusters with $n > 3$ excited at 4.65 eV to autodetachment. This assignment is supported by the observation that the intensity of feature A is largely complementary to that of the pump−probe feature. The time-dependent intensities result from competition between detachment of the excited state by the probe pulse vs autodetachment from the excited state, as indicated in eq 7.

$$A^- \xrightarrow{h\nu_{pu}} A^-* \xrightarrow{\tau_d} A + e^- \quad [eKE \sim 0]$$
$$\xrightarrow{t,h\nu_{pr}} A + e^- \quad [eKE = h\nu - VDE] \quad (7)$$

At short pump−probe delays, the probe pulse depletes the excited state population and hence the autodetachment signal, whereas at delays much longer than the autodetachment lifetime, no depletion occurs because the excited state has already decayed by autodetachment. Similar effects were seen and analyzed in detail in a recent study of water cluster anions in our group.[42] Hence the time constant τ_d in eq 2 reflects the autodetachment lifetime, and we attribute decay of the population excited through the CTTS channel to excited state autodetachment, as was postulated by Lehr et al.[20]

For cluster sizes $n = 8-10$, the dynamics are more complicated. We interpret the major decay channel, governed by τ_{d2}, as autodetachment as it is consistent with the slow recovery of I_A observed for these larger clusters. We note that the time constants τ_{d1} for the minor channel are generally quite close to those of τ_3 in Table 2.

5.2. Time-Dependent VDEs. The time-dependent VDEs, summarized in Table 2, yield detailed information on the excited state dynamics before autodetachment occurs. All clusters with $n \geq 5$ show time-dependent VDEs similar to those shown in Figure 6 for $I^-(D_2O)_9$: the VDE drops by ΔE_1 at very early times to VDE_{min}, rises by ΔE_2 to VDE_{max}, and then drops by about 50 meV (ΔE_3) to its final value, VDE(∞). The time scales τ_2 for the ΔE_2 shift vary from 200 fs for $I^-(H_2O)_4$ to 1430 fs for $I^-(D_2O)_{10}$, while those for the final shift, ΔE_3 are considerably longer, ranging from 25 ps for $I^-(H_2O)_5$ to 90 ps for $I^-(D_2O)_{10}$. The ΔE_2 shifts are similar to those reported previously,[20,22] but the earlier work was not carried out at sufficiently long pump−probe delays to observe the ΔE_3 shifts. The time scale of the second energy shift is consistently ~1.2 times faster in H_2O clusters than in D_2O clusters for $n > 6$, which suggests that this shift is due to solvent dynamics. The reason for its appearance only in larger clusters is unclear, but may be simply a function of increasing complexity of the solvent network. The lack of any consistent isotope effect in τ_3, on the other hand, may point to iodide motion. The dynamics responsible for the two shifts are discussed further in the paragraphs following.

The earliest energy shift, ΔE_1, is observed consistently in all the clusters ($n \geq 5$) considered here. The time scale for this shift is on the order of the cross-correlation of the pump and probe pulses, about 180 fs, and thus is essentially instantaneous at the temporal resolution of our experiment. We speculate that it represents rapid excited state dynamics involving little or no solvent motion, possibly analogous to the formation of a "contact pair" between the excited electron and neutral I atom that occurs in aqueous iodide solution, for which the time scale of formation is 200 fs.[16]

In the original study by Lehr et al.,[20] the shift ΔE_2 was interpreted in terms of rearrangement of the solvent molecules to stabilize the excess electron created by CTTS excitation of the cluster. This interpretation was questioned by Chen and Sheu,[18,24] who proposed instead that the observed shift resulted

from the neutral I atom leaving the cluster, with the sign of the shift reflecting the repulsive interaction between the I atom and the diffuse orbital for the excited electron. More recent calculations by Jordan[26] and Peslherbe [27] have indicated that the initial dynamics after CTTS excitation do involve solvent motion, in agreement with our interpretation, but that the I atom does leave the cluster at some point. The energetics associated with I atom and solvent motion have also been considered in electronic structure calculations by Kim and co-workers.[19,28] Hence a complete picture of the excited state dynamics requires understanding the presumably coupled motions of the water molecules and the I atom.

With this background in mind, there are two limiting interpretations of the VDE shifts that need to be considered carefully. The first is that ΔE_2 and ΔE_3 correspond to solvent stabilization of the excess electron and dissociation of the cluster to $I + (H_2O)_n^-$, respectively, with the overall mechanism given by

$$I^-(H_2O)_n \xrightarrow{h\nu_{pu}} I\cdot(H_2O)_n^-* \xrightarrow{\tau_2,\Delta E_2} I\cdot(H_2O)_n^- \xrightarrow{\tau_3,\Delta E_3} I + (H_2O)_n^- \quad (8)$$

This mechanism is essentially an extension of our original proposal, with an additional time constant associated with dissociation of the I atom. Alternatively, ΔE_2 could represent the stabilization of the cluster from the I atom leaving, while ΔE_3 represents subsequent dynamics associated with the bare water cluster anion:

$$I^-(H_2O)_n \xrightarrow{h\nu_{pu}} I\cdot(H_2O)_n^-* \xrightarrow{\tau_2,\Delta E_2} I + (H_2O)_n^-* \xrightarrow{\tau_3,\Delta E_3} I + (H_2O)_n^-, I + (H_2O)_{n-1}^- + H_2O \quad (9)$$

These two mechanisms are extensions of the so-called "solvent-driven" and "iodine-driven" models of relaxation in these clusters.[27] There are fairly significant differences implied by the two mechanisms. For example, since $\Delta E_3 \equiv VDE(\infty) - VDE_{max} < 0$, eq 8 implies that there is an attractive interaction between the I atom and $(H_2O)_n^-$ moiety, resulting in a lower VDE (by ~50 meV) once the I atom has departed. In contrast, since $\Delta E_2 > 0$, eq 9 implies a fairly repulsive interaction between the I atom and $(H_2O)_n^-$*, resulting in an increase in VDE as high as 400 meV (for $n = 8$) when the I atom leaves the cluster. In addition, the last step in eq 9 requires dynamics in the bare water cluster anion that lower, rather than raise, the VDE; one possible mechanism is cluster fragmentation.

We now consider the two mechanisms in more detail. Figure 7b provides an important point of reference in their evaluation, comparing the minimum, maximum, and final VDEs from our experiment to those of the two isomers of $(H_2O)_n^-$ anions. It shows that, for all clusters studied here except $n = 10$, VDE_{min} lies very close to the VDE of the more weakly bound water cluster anions. For clusters with $6 \leq n \leq 9$, VDE_{max} overshoots the VDE of the more strongly bound $(H_2O)_n^-$ cluster, but this difference narrows significantly for VDE(∞). Since VDE_{min} is reached within the cross-correlation of the pump and probe pulses, presumably before the heavy I atom has had much chance to do anything, the VDE_{min} values suggest that, just after excitation, the cluster can be described by the less stable form of the water cluster anion interacting very weakly with the I atom. We note that Kim and co-workers[19,43] have calculated the geometries of many $I^-(H_2O)_n$ and $(H_2O)_n^-$ clusters, and indeed have found in several cases that the solvent network in the lowest energy $I^-(H_2O)_n$ cluster is similar to that of a $(H_2O)_n^-$ structure whose VDE matches the lower experimental value.

Moving on to VDEs at later times, if the shift ΔE_2 is primarily from solvent stabilization of the excess electron, as implied by eq 8, then we would expect VDE_{max} to be the VDE of the more stable water cluster plus whatever additional interactions arise from the I atom, with an attractive interaction raising VDE_{max} and a repulsive interaction lowering it. The "overshoot" with respect to the VDE of the more stable $(H_2O)_n^-$ isomer is consistent with VDE_{max} corresponding to this isomer attractively bound to the I atom, as is the drop in VDE at the longest times, i.e., VDE(∞), if the last step in the dynamics is the I atom leaving the cluster. The dissociation step is driven by the internal energy released by solvent stabilization of the excess electron. However, the discrepancy in VDE and width exemplified in Figure 7a between the pump−probe PE spectrum, at longest times, when the I atom has presumably left the cluster, and that of the one-photon PE spectrum for the bare cluster ion, is somewhat puzzling.

There are several aspects of the alternate mechanism (eq 9) that are also consistent with our results. According to the calculations by Kim,[28,29] the $I^-(H_2O)_6$ CTTS state is stabilized by about 0.2 eV if the I atom moves from its original position, about 3.5 Å away from the nearest O atom, to a shallow minimum (~0.02 eV) at 10 Å. Assuming the I atom were to leave the cluster at this point, the VDE would have increased by approximately 0.2 eV (assuming the neutral surface to be flat along the dissociation coordinate); this energy is close to (but smaller than) ΔE_2 for $I^-(H_2O)_6$. The subsequent drop in the VDE by 50 meV would then be attributed to fragmentation of the water cluster anion, as indicated in eq 9.

Quantitative aspects of this mechanism are less satisfactory. The stabilization gained from I atom motion would have to double from $n = 6-8$ to match the experimental values of ΔE_2. Moreover, if ΔE_2 is due purely to iodine motion, it is difficult to understand why there should be any isotope effect in τ_2 for the larger clusters. Finally, the VDEs of $(H_2O)_n^-$ clusters do not increase evenly or even monotonically with cluster size. Hence, the independence of the 50 meV shift, ΔE_3, from cluster size is not consistent with loss of a water molecule from a bare water cluster anion.

Overall, it appears that "solvent-driven" dynamics are more consistent with the experimental results than "iodine-driven" dynamics. However, it does appear that I atom motion stabilizes the electronically excited cluster, so it is quite possible that the large increase in VDE, ΔE_2, represents a combination of solvent stabilization and iodine motion (but not dissociation), as was indicated in the simulations on $I^-(H_2O)_3$ by Peslherbe.[27] The assignment of the final shift, ΔE_3, to I atom loss is reasonable, but it requires the existence of a potential energy minimum of at least 50 meV on the surface representing the interaction of an I atom with a $(H_2O)_n^-$ cluster. Kim has already found a 20 meV well for the $n = 6$ cluster,[29] so the existence of a slightly deeper well from a more extensive search would not be too surprising. This attractive interaction is also consistent with condensed phase observations which require a 70−100 meV potential well[15,17] stabilizing the $(I{:}e^-)_{aq}$ contact pair to model recombination dynamics.

Neither mechanism provides an obvious explanation for the differences between the long-time pump−probe and one-photon spectra in Figure 7. However, the bare cluster anion formed by I atom dissociation is considerably hotter than that formed in a free jet expansion. As a result, it may represent a mixture of multiple, nearly degenerate isomers with a range of VDEs,

thereby yielding a similar but noticeably different PE spectrum than that of the cooled bare cluster ion.

5.3. Relationship between Excited State Lifetimes and VDE Shifts. The experimental results described above cover two classes of time-dependent phenomena: the lifetime of the excited state with respect to autodetachment, τ_d, and the time constants τ_2 and τ_3 associated with excited state dynamics. These time constants are coupled to one another in the sense that we can only observe τ_2 and τ_3 if they are shorter than τ_d; once the excited state has autodetached, the experiment is no longer able to follow any excited state dynamics. In fact, Tables 1 and 2 show that this condition is satisfied for all clusters with $n \geq 5$; the autodetachment lifetime increases much more rapidly with cluster size than τ_2 and τ_3. Hence, the time constant for the I atom leaving the cluster is shorter than that for autodetachment, implying that the autodetaching species is highly excited $(H_2O)_n^-$, not $I\cdot(H_2O)_n^-$. For the $n = 4$ and 3 clusters, no evidence for the shift ΔE_3 is seen. We interpret this result to mean that autodetachment occurs before the I atom leaves the cluster.

5.4. Comparison with Bulk Processes. The dynamics following CTTS excitation in aqueous iodide solution proceed in several stages:[16,17] (1) rapid electron ejection to the solvent in close proximity to the parent halogen to form a contact pair within ~200 fs, (2) equilibration of the $I{:}e^-$ contact pair involving relaxation of the surrounding solvent, with a time constant on the order of 1 ps, (3) recombination of the electron with the iodine atom with a time constant of ~33 ps, and (4) diffusive escape of the electron from the contact pair with a time constant of 70 ps (upper limit). We note that dynamics associated with step 2 are reported by Iglev[17] but not in the earlier work by Kloepfer;[16] the origin of this discrepancy is as yet unresolved.

There are similarities between the time scales seen in our experiment and those in solution. We observe the two shifts, ΔE_1 and ΔE_2, in the time-dependent VDEs on time scales of <150 fs and 0.2−1 ps, suggesting analogies to steps 1 and 2 above. We then observe slower dynamics in the VDEs with time constants τ_3 on the order of tens of picoseconds, similar to those associated with the bulk in steps 3 and 4. However, there are clearly significant differences between the cluster and bulk experiments, not the least of which is that the iodide anion resides at the surface of an $I^-(H_2O)_n$ cluster, resulting in excitation into an orbital that differs from that in the bulk in terms of both its size and shape and its interaction with the solvent molecules.[5] Questions also arise regarding correspondences between the processes assigned to longer time dynamics in the clusters and in solution, although one could argue that I atom dissociation, leaving a bare water cluster anion, is analogous to dissociation of the contact pair.

Recent studies of water cluster anions have shown it to be necessary to examine substantially larger clusters than those studied here in order to observe dynamics that extrapolate to those observed for the bulk hydrated electron.[44,45] The same considerations may apply to halide water clusters as well, and studies of larger clusters of this type are currently underway in our laboratory.

6. Summary

Figure 8 summarizes our interpretation of the dynamics of clusters $n = 5-10$. Excitation by the pump laser transfers the excess electron to the solvent in a diffuse, dipole-bound state, $(I\cdot(H_2O)_n^-)^*$. Subsequent solvent rearrangement on a time scale of a few picoseconds (τ_2) reduces the iodine−electron interaction and localizes the electron on the water cluster in a more tightly bound state, $I\cdot(H_2O)_n^-$, resulting in stabilization by several hundred millielectronvolts (ΔE_2). At long times ($\tau_3 \sim$ tens of picoseconds), a slight destabilization ($\Delta E_3 \sim 50$ meV) occurs, which we suggest is caused by the iodine atom physically leaving the cluster. Autodetachment from the excited state occurs concurrently, but on a much slower time scale than the other dynamics ($\tau_d \sim$ tens to thousands of picoseconds).

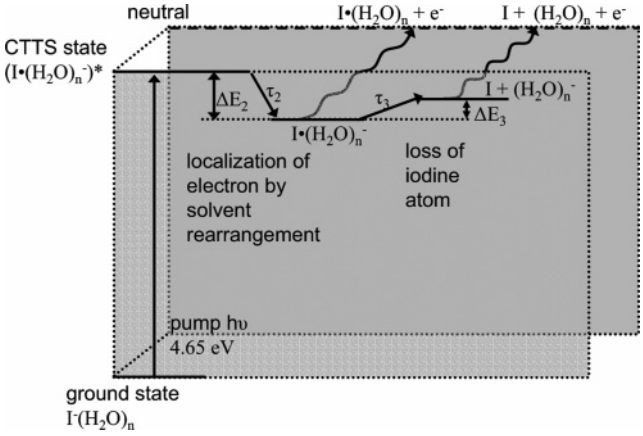

Figure 8. Summary of the observed dynamics for $n = 5-10$. Wavy arrows indicate the autodetachment pathway available to the excited electron. The horizontal axis and the axes in and out of the plane of the page indicate motion along different solvent coordinates.

Acknowledgment. This research was funded by the National Science Foundation under Grant CHE-0350585. The authors thank Ori Cheshnovsky for providing the pulsed valve used in some of these measurements. D.M.N. thanks Jack Simons for teaching him about autodetachment in the 1980s.

References and Notes

(1) Keutsch, F. N.; Saykally, R. J. *Proc. Natl. Acad. Sci. U.S.A.* **2001**, *98*, 10533.
(2) Shin, J. W.; Hammer, N. I.; Diken, E. G.; Johnson, M. A.; Walters, R. S.; Jaeger, T. D.; Duncan, M. A.; Christie, R. A.; Jordan, K. D. *Science* **2004**, *304*, 1137.
(3) Robertson, W. H.; Johnson, M. A. *Annu. Rev. Phys. Chem.* **2003**, *54*, 173.
(4) Serxner, D.; Dessent, C. E. H.; Johnson, M. A. *J. Chem. Phys.* **1996**, *105*, 7231.
(5) Bradforth, S. E.; Jungwirth, P. *J. Phys. Chem. A* **2002**, *106*, 1286.
(6) Franck, J.; Scheibe, G. *Z. Phys. Chem., Stoechiom. Verwandschaftsl.* **1928**, *139*, 22.
(7) Jortner, J.; Ottolenghi, M.; Stein, G. *J. Phys. Chem.* **1964**, *68*, 247.
(8) Blandamer, M. J.; Fox, M. F. *Chem. Rev.* **1970**, *70*, 59.
(9) Long, F. H.; Lu, H.; Shi, X.; Eisenthal, K. B. *Chem. Phys. Lett.* **1990**, *169*, 165.
(10) Gauduel, Y.; Gelabert, H.; Ashokkumar, M. *Chem. Phys.* **1995**, *197*, 167.
(11) Sheu, W.; Rossky, P. J. *J. Am. Chem. Soc.* **1993**, *115*, 7729.
(12) Staib, A.; Borgis, D. *J. Chem. Phys.* **1996**, *104*, 4776.
(13) Staib, A.; Borgis, D. *J. Chem. Phys.* **1996**, *104*, 9027.
(14) Kloepfer, J. A.; Vilchiz, V. H.; Lenchenkov, V. A.; Bradforth, S. E. *Chem. Phys. Lett.* **1998**, *298*, 120.
(15) Kloepfer, J. A.; Vilchiz, V. H.; Lenchenkov, V. A.; Chen, X.; Bradforth, S. E. *J. Chem. Phys.* **2002**, *117*, 766.
(16) Kloepfer, J. A.; Vilchiz, V. H.; Lenchenkov, V. A.; Germaine, A. C.; Bradforth, S. E. *J. Chem. Phys.* **2000**, *113*, 6288.
(17) Iglev, H.; Trifonov, A.; Thaller, A.; Buchvarov, I.; Fiebig, T.; Laubereau, A. *Chem. Phys. Lett.* **2005**, *403*, 198.
(18) Chen, H.; Sheu, W. *J. Am. Chem. Soc.* **2000**, *122*, 7534.
(19) Lee, H. M.; Kim, K. *J. Chem. Phys.* **2001**, *114*, 4461.
(20) Lehr, L.; Zanni, M. T.; Frischkorn, C.; Weinkauf, R.; Neumark, D. M. *Science* **1999**, *284*, 635.
(21) Davis, A. V.; Zanni, M. T.; Frischkorn, C.; Neumark, D. M. *J. Electron Spectrosc. Relat. Phenom.* **2000**, *108*, 203.
(22) Frischkorn, C.; Zanni, M. T.; Davis, A. V.; Neumark, D. M. *Faraday Discuss.* **2000**, 49.

(23) Zanni, M. T.; Frischkorn, C.; Davis, A. V.; Neumark, D. M. *J. Phys. Chem. A* **2000**, *104*, 2527.
(24) Chen, H.; Sheu, W. *Chem. Phys. Lett.* **2001**, *335*, 475.
(25) Chen, H.; Sheu, W. *Chem. Phys. Lett.* **2002**, *353*, 459.
(26) Vila, F. D.; Jordan, K. D. *J. Phys. Chem. A* **2002**, *106*, 1391.
(27) Timerghazin, Q. K.; Peslherbe, G. H. *J. Am. Chem. Soc.* **2003**, *125*, 9904.
(28) Lee, H. M.; Kim, K. *Mol. Phys.* **2004**, *102*, 2485.
(29) Lee, H. M.; Suh, S. B.; Kim, K. *J. Chem. Phys.* **2003**, *119*, 7685.
(30) Bragg, A. E.; Wester, R.; Davis, A. V.; Kammrath, A.; Neumark, D. M. *Chem. Phys. Lett.* **2003**, *376*, 767.
(31) Even, U.; Jortner, J.; Noy, D.; Lavie, N.; Cossart-Magos, C. *J. Chem. Phys.* **2000**, *112*, 8068.
(32) Wiley, W. C.; McLaren, I. H. *Rev. Sci. Instrum.* **1955**, *26*, 1150.
(33) Eppink, A. T. J. B.; Parker, D. H. *Rev. Sci. Instrum.* **1997**, *68*, 3477.
(34) Dribinski, V.; Ossadtchi, A.; Mandelshtam, V. A.; Reissler, H. *Rev. Sci. Instrum.* **2002**.
(35) Reid, K. L. *Annu. Rev. Phys. Chem.* **2003**, *54*, 397.
(36) Markovich, G.; Pollack, S.; Giniger, R.; Cheshnovsky, O. *J. Chem. Phys.* **1994**, *101*, 9344.
(37) Kim, J.; Becker, I.; Cheshnovsky, O.; Johnson, M. A. *Chem. Phys. Lett.* **1998**, *297*, 90.
(38) Coe, J. V.; Lee, G. H.; Eaton, J. G.; Arnold, S. T.; Sarkas, H. W.; Bowen, K. H.; Ludewigt, C.; Haberland, H.; Worsnop, D. R. *J. Chem. Phys.* **1990**, *92*, 3980.
(39) Shin, J. W.; Hammer, N. I.; Headrick, J. M.; Johnson, M. A. *Chem. Phys. Lett.* **2004**, *399*, 349.
(40) Hammer, N. I.; Roscioli, J. R.; Johnson, M. A. Manuscript in preparation.
(41) Castleman, A. W., Jr.; Bowen, K. H., Jr. *J. Phys. Chem.* **1996**, *100*, 12911.
(42) Bragg, A. E.; Verlet, J. R. R.; Kammrath, A. E.; Griffin, G.; Cheshnovsky, O.; Neumark, D. M. Submitted for publication in *J. Am. Chem. Soc.*
(43) Lee, H. M.; Lee, S.; Kim, K. S. *J. Chem. Phys.* **2003**, *119*, 187.
(44) Bragg, A. E.; Verlet, J. R. R.; Kammrath, A.; Cheshnovsky, O.; Neumark, D. M. *Science* **2004**, *306*, 669.
(45) Paik, D. H.; Lee, I. R.; Yang, D. S.; Baskin, J. S.; Zewail, A. H. *Science* **2004**, *306*, 672.